This is an open access article published under an ACS AuthorChoice License, which permits copying and redistribution of the article or any adaptations for non-commercial purposes.

ACS OMEGA

http://pubs.acs.org/journal/acsodf

Article

Biodiesels Manufactured from Different Feedstock: From Fuel Properties to Fuel Atomization and Evaporation

Phuong X. Pham,* Kien T. Nguyen, Thin V. Pham, and Vu H. Nguyen

Cite This: *ACS Omega* 2020, 5, 20842−20853

Read Online

ACCESS | Metrics & More | Article Recommendations

ABSTRACT: Different from fossil diesel, biodiesels can be manufactured from different sources of biomass or animal fat. Each biodiesel manufactured from a certain feedstock consists of different fatty acid methyl esters (FAMEs). Its FAME types and fractions are unique and are solely controlled by the mother feedstock and not the manufacturing process. One key feature that makes biodiesels different from their fossil counterparts is the oxygen contained in biodiesels. The oxygen content, FAME types, and FAME fractions vary in a wide range among biodiesels made from different feedstock and this in turn affects the fuel properties and physical processes, including atomization and evaporation. An extensive analysis has been successfully carried out in this study to examine the role of oxygen content, carbon chain length, and unsaturation degree in different biodiesels and the influence of FAMEs on key fuel properties (heating value, cetane number, viscosity, and surface tension). Furthermore, some useful information related to (i) the morphology and density of fuel fragments derived close to the nozzle exit and (ii) drop evaporation is reported. The atomization characteristics are experimentally observed using a high-speed imaging technique developed earlier, while the evaporation study is theoretically conducted using the well-known D-square model. It shows that the oxygen in the biodiesel is directly linked to the carbon chain length and the number of double bonds in the fuel molecules as well as to the key fuel properties. The viscosity of biodiesels and their constituents has a certain impact on the morphology and population of fuel fragments derived in the breakup zone, while the thermal properties have a significant effect on biodiesel evaporation. The dependence of fuel properties on atomization at the downstream locations of the spray, where the breakup process has completed, is minimal.

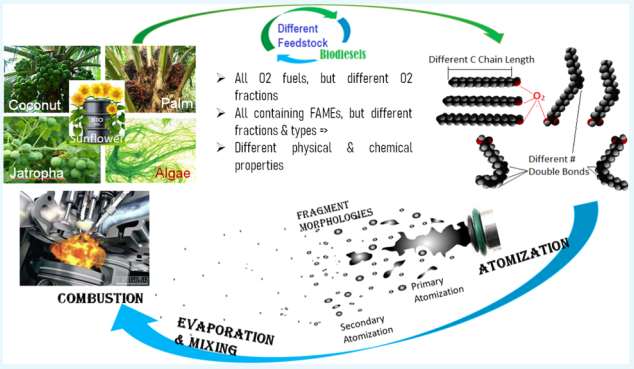

1. INTRODUCTION

With the limitation of crude-oil reserves and the dramatic increase of energy and feedstock resource demand for the transportation sector,[1] it is crucial to explore alternative fuels to reduce the dependency on fossil fuels.[2−5] It was estimated that 60% of 70 million crude-oil barrels was consumed daily by roughly one billion vehicles operating worldwide in 2014[6,7] and that this number will rise to more than 100 million barrels by 2040.[8] Alternative fuels including biodiesels and alcohols manufactured from biomass are potential candidates to partly replace fossil fuels.[9,10] The energy derived from vegetable oils and animal fats is promising to fuel the world's fleet and this helps not only to reduce the fossil-oil dependency but also to improve energy utilization efficiency and decrease environmental pollution.[10,11] One of the key characteristics of fuels derived from vegetable oils is that the fuels contain oxygen in their molecules and this feature makes them special compared to their fossil counterparts. In autoignition engines, the fuel oxygen enhances the quality of combustion in the fuel spray's reaction zone, where the fuel−air mixture is rich (lack of oxygen).[12,13] Another key characteristic of vegetable oil-based biofuels is that each fuel made from a certain feedstock has its unique profiles that are solely determined by the feedstock. This leads to differences in the properties of biofuels manufactured from different feedstock and as such differences in their atomization, evaporation, combustion, and emission characteristics.[14,15] A coconut-based biodiesel, for example, benefits from its low viscosity and high cetane number (CN) but its drawback is the low calorific value.[16] A biodiesel manufactured from algae, a promising future biofuel,[17] has a higher calorific value and CN compared to those of the coconut-based fuel but the algae-based fuel's viscosity is higher due to its longer carbon chain length.[16] The broad variation in physical and chemical properties of biodiesels manufactured

Received: May 5, 2020
Accepted: July 27, 2020
Published: August 10, 2020

Downloaded via 220.231.117.237 on August 26, 2020 at 23:52:20 (UTC).
See https://pubs.acs.org/sharingguidelines for options on how to legitimately share published articles.

© 2020 American Chemical Society

https://dx.doi.org/10.1021/acsomega.0c02083
ACS Omega 2020, 5, 20842−20853

from different feedstock needs to be addressed when producing biodiesels and utilizing them in heat engines.[5,18] The variation adds more complexity to the physical and chemical processes that liquid fuels involve in during one engine cycle. Therefore, the fuel properties should be controlled, if possible, to advance the processes as such to improve fuel atomization, evaporation, and combustion quality and to decrease exhaust pollutants. This article aims to examine the properties of biodiesels made from different feedstock and to briefly investigate the influence of fuel properties on important physical processes, including the atomization, morphology, and density of fuel fragments derived in the near-field of the nozzle exit) and evaporation. Correlations between the key biodiesel features (e.g. fuel oxygen content, molecular weight, carbon chain length, and number of double bonds) and important fuel properties (e.g. heating value, viscosity, surface tension, and cetane number) are developed. The morphology and density of fuel fragments derived in primary and secondary atomization zones and droplet evaporation rates are reported for a wide range of biodiesels made from different feedstock. This may provide useful information for optimizing future biodiesels to utilize in heat engines. For example, mixing a biodiesel made from coconut oil (having high CN but low heating value) and a fuel manufactured from algae (high heating value but low cetane number) may provide a better fuel to power heat engines.

Biodiesels are mixtures of different fatty acid methyl esters (FAMEs) produced from biomass or animal fat through a well-known process called transesterification with the aid of methanol as a solvent.[5] The profile of FAMEs is a unique characteristic of each feedstock and cannot be controlled during the transesterification process (ASTM-D6751 or EN14214).[5] The mono-FAMEs always have two oxygen atoms in their molecule. However, their carbon chain lengths vary over a wide range from 8 to 25 and the number of double bonds in their chain can range from 0 to 6.[5] The variation in chain length and number of double bonds leads to a variation in the oxygen fraction of their molecule. Although oxygen in the fuel could enhance fuel reactivity, it results in a lower calorific value.[5,19−23] At the same air−fuel equivalence ratio, mixtures of biodiesels (with oxygen in the molecule) and air are always leaner compared to mixtures of fossil counterparts (without oxygen in the molecule) and air.[13,24]

Different from gaseous fuels, combustion of liquid counterparts involves complex physical processes such as atomization, droplet−droplet collision, vaporization, and mixing. In general, the purpose of atomization studies is to determine appropriate atomizing regimes for (i) decreasing the droplet size and therefore increasing the liquid surface area, which is necessary to improve fuel evaporation and mixing, and (ii) obtaining an appropriate spray structure for decreasing the wall wetting issue and therefore improving combustion and emission quality. In compression ignition engines, a liquid fuel such as diesel or a biodiesel is sprayed into the combustion chamber and atomized to form small drops near the nozzle exit. The liquid jet is broken up and usually forms a cone-shaped spray at the nozzle exit and its viscosity and surface tension have significant effects on the primary as well as secondary breakup quality.[23,25]

Studies of fuel atomization have been performed using (i) practical systems such as IC engines;[26] (ii) constant-volume chambers or open environment systems using practical injectors;[27,28] or (iii) shock tubes, cross-flow air streams, and drop towers.[29] Approach (i) can help to observe only the macroscopic information of the atomization in real systems, such as spray angle and penetration, while approach (ii) can give more additional information such as the Sauter mean diameter (SMD). In the first two approaches, the spray is too dense and the process is too fast so that the current diagnostic capabilities are challenged. The last method of flow in a cross stream of air is employed in this work. It is a fundamental approach that is capable of qualifying and quantifying microscopic parameters such as breakup length and time, breakup mechanism, and breakup regimes. It is to be noted that there is a difference in selecting the control parameters among these methods. Approaches (i) and (ii) are usually performed with the same working conditions of the systems (such as engine speed and load, injection pressure, and temperature), while method (iii) uses dimensionless parameters such as Weber (*We*), Ohnesorge (*Oh*), and Reynolds numbers (*Re*). The differences in liquid properties such as viscosity and surface tension may be accounted for using the nondimensional parameters such as *We*, *Oh*, and *Re* mentioned above, all of which are used to generate regime diagrams that characterize the various atomization modes. It is also to be noted that the tests carried out at given or fixed temperatures and pressures (usually ambient conditions) in the fundamental studies are not identical to practical conditions and a question commonly raised is whether the results are relevant to practical conditions.[30] In a working engine, atomization occurs close to the injector tip zone, which is cooled by the fuel passing through so that atomization in a real engine is not at an excessively high temperature.[30] In addition, pressure does not affect the fuel surface tension extensively.[31]

Knowledge of drop evaporation and burning is relevant to many practical combustion systems, including heat engines. Although in such combustion devices, the spray combustion process is dominant rather than monodroplet evaporation and burning, an understanding of the latter is essential as this supplies a submodel for the complex processes occurring in the systems. A thorough understanding of the physicochemical processes in heat engines is now pressing, particularly with the advent of biodiesel fuels where the variability of the fuel constituents could affect these processes. A number of models developed for monocomponent-droplet heating and evaporation of various complexities have been introduced (for example, D-square, Maxwell, and Stefan−Fuchs; Abramzon and Sirignano; Yao, Abdel−Khalik, and Ghiaasiaan; and Tonini and Cossali Models) and the reader is directed to refs 32−34 for further information. The D-square law is the most convenient with an acceptable uncertainty[35] for estimating the evaporation rate of different fuels, including biodiesels.

A number of studies on biodiesels and excellent reviews on this topic (both fundamental studies and biodiesel utilization) can be found in the literature.[18,20,36−48] The common findings noted in the current literature include the following: (i) biodiesels can be made from different feedstock and could be a potential candidate to partly replace fossil diesel used in compression ignition engines[49,50] and these biofuels could be blended with fossil diesel with or without additives,[51−53] (ii) biodiesels have a higher cetane number but a lower calorific value and higher viscosity compared to fossil diesel,[5,54] and (iii) fueling engines with biodiesels can help to decrease specific particulate matter in mass basic, while the effect of biodiesels on NO_x formation and particle number and size

https://dx.doi.org/10.1021/acsomega.0c02083
ACS Omega 2020, 5, 20842−20853

Table 1. Constituents and Important Properties of Testing Biodiesels

constituents' mass fraction						
	BF1	BF2	BF3	BF4	PB	*D*
C8:0	52.16					
C10:0	46.38	0.17				
C12:0	1.38	47.8	0.1			
C14:0		18.9	0.06	0.03		
C15:0			0.03	0.02		
C16:0		10.2	21	4.45	28.09	
C16:1				0.12		
C17:0			0.06	0		
C18:0		2.55	9.47	2.53	9.53	
C18:1				0.38	43.47	
C18:1cis		18.5	58.7	68.1		
C18:1trans				3.96		
C18:2		1.76	9.98	18.7	18.02	
C20:0		0.08	0.3	0.49		
C20:1			0.24	1.03		
C22:0		0.03	0.03	0.17		
glycerol	0.08					

important properties						
	BF1	BF2	BF3	BF4	PB	*D*
average C atoms	9.5	14.8	18.3	18.7	18.94	13.78
average H atoms	19.7	28.3	35.3	35.3	36.03	26.42
stoi. AFR, wt	11.12	12.05	12.50	12.48		14.5
oxygen content (wt %)	19.29	13.47	11.14	10.96	10.84	
iodine value	1 max	8	65	105		
saponif. number	330	233	195	185		
rel. density, at 20 °C (kg/m^3)	0.877	0.871	0.873	0.879	0.871	0.848
heating value (MJ/kg)	35.35	38.66	39.87	38.07	38.10	43.4
cetane value	42	69.8	65.4	59	66.9	48.4
viscosity (kPa s)	1.71	3.81	4.32	4.65	6.16	3.2
surface tension (N/m) × 10^3	26.1	28.4	29.9	29.96	24.82[30]	23

distribution is not fully understood.[18,55] Further investigations of physical and chemical properties of biodiesels made from different feedstock are essential to have a comprehensive understanding of the engine performance when operating with biodiesels. The impact of FAME profiles, especially oxygen content, on the properties of biodiesels made from different feedstock, and the influence of fuel properties on fuel atomization and evaporation, according to the authors' knowledge, is not quite clear in the literature.

In this current work, a thorough study on biodiesels manufactured from different feedstock, biodiesel constituents (FAMEs), and some other oxygenated fuels, including ethers and alcohols, is conducted. First, the influence of oxygen contained in a wide range of biodiesels from the first to the third biodiesel generations on their important properties is explained. Then, some characteristics of fuel atomization and evaporation are also given, which aims to provide additional information for a deeper understanding of physical processes occurring in cycles of autoignition engines when operating with biodiesels.

2. METHODOLOGY

2.1. Selection of Biodiesels. In this study, five different biodiesels produced from different feedstock and their blends with fossil diesel are examined from different angles, covering fuel properties, fuel atomization, and evaporation. In our previous work,[16] the first four interesting biodiesels (BF1, BF2, BF3, and BF4, respectively) were carefully selected to study the influence of biodiesel molecular profiles on atomization, combustion, and emission. Palmer and coconut-based oils were used as the main feedstock to produce BF1 and BF2, respectively; BF3 was manufactured from pale-based oil, while BF4 is a canola-based oil liquid.[56] In our previous projects,[16,25,57,58] BF1 and BF2 were chosen to represent saturated biodiesels; however, BF1 has a shorter carbon chain length than BF2, which has a medium carbon chain length. BF3 and BF4 have long and similar carbon chain lengths but different unsaturation degrees. BF3 is partially unsaturated, while BF4 is almost fully unsaturated. The fifth biodiesel is a novel biodiesel manufactured from residues of a palm cooking-oil production process (not used cooking oil). The residues were found to be rich in FAMEs, and this interesting feedstock was successfully transesterified to produce the biofuel using a process called triple cycles of heterogeneous catalysis.[59] Our previous reports[21,60,61] have tested this palm oil-based fuel in autoignition engines. As a palm oil-based biodiesel, this fuel is called PB in this work.

The five biodiesels (BF1−BF4 and PB) selected here cover a wide range of fuels made from variable feedstock used to manufacture biodiesels from the first to the third generations.[16] Different biodiesel−diesel blends, from pure diesel (B0) to pure biodiesel (B100), are also tested in this study. Oxygen contained in these five biodiesels covers a wide range from 10 to 20% by weight and as such the oxygen content in their

https://dx.doi.org/10.1021/acsomega.0c02083
ACS Omega 2020, 5, 20842−20853

blends varies from 0 to 20%. It is noted that the oxygen content in common biodiesels varies within a range of 10−12%. However, the oxygen contents of some biodiesels, including palmer, BF1 in this study, coconut-based oil, BF2 in this study, and algae-based biodiesels, are much higher. Additionally, biodiesels are mixtures of different fatty acid methyl esters (FAMEs), which have a wide range of oxygen content varying between 10 and 20% depending on the FAME molecular structure (carbon chain length and number of double bonds).

The important properties of these five biodiesels along with fossil diesel are shown in Table 1, and the reader is directed to our previous work[16,62] for properties of biodiesel−diesel blends. The compositions and properties of biodiesels shown in Table 1 have been carefully measured using different standardized methodologies.[16] FAME compounds of the biodiesels were tested using a gas chromatography mass spectrometry (GCMS) analysis.[16] Higher heating values of these biodiesels were tested using bomb calorimeters.[62] Biodiesel viscosity was measured using the Brookfield DV-III Rheometer and following the ASTM D445 standard test method. More details on the viscosity testing can be found in refs 16, 62, 63. Cetane numbers of BF1−BF4 were tested using a BASF (Badische Anilin-und Soda Fabrik) engine operating under DIN-51773 German standard,[16,64] while the CN of PB was measured using a cetane testing engine.[21,22] The properties of the FAMEs shown in Table 1 are available elsewhere,[5] and properties of ethers and alcohols used in this work can be found in refs 20, 65.

2.2. Selection of Biodiesel Constituents: Fatty Acid Methyl Esters. To examine the role of oxygen in fuel properties, along with the biodiesels and their blends reported in Section 2.1, monosaturated and unsaturated FAMEs (biodiesels' constituents) and some oxygenated fuels (ethers and alcohols) are also included here. Pure or mono-FAMEs used here include eight saturated mono-FAMEs (C8:0, C12:0, C14:0, C16:0, C18:0, C20:0, C22:0, and C24:0) and seven unsaturated mono-FAMEs (C16:1, C18:1, C18:2, C18:3, C20:1, C22:1, and C24:1). C*x*:*y* represents one FAME and it means that the FAME molecule includes *x* carbon atoms and *y* number of double bonds and as such *x* represents the FAME carbon chain length, while *y* is linked to the FAME unsaturation degree. The saturated and unsaturated mono-FAMEs used for analysis here are common constituents of biodiesels. The properties of these mono-FAMEs are given in ref 5.

The ethers are included here for a comparison purpose. Ethers selected include diethylene glycol dimethyl ether (DGM (CH3O(CH2)2O(CH2)2OCH3)), ethylene glycol mono-*n*-butyl ether (ENB (CH3(CH2)3O(CH2)2OH)), 2-ethylhexyl acetate (EHA (CH3(CH2)7O(CO)CH3)), and di-*n*-butyl ether (DBE(CH3CH2)3OCH3(CH2)3). They are known as fuel additives to enhance fuel reactivity.[20] In addition, three alcohols (ethanol, methanol, and butanol) are also included here as they are oxygenated fuels, which can be used as solvents in the transesterification process to produce biodiesels, so it is good to examine them along with biodiesels. The properties of FAMEs, ethers, and alcohols selected here are taken from the literature.[5,20]

2.3. Experimental Setup for Examining Primary and Secondary Atomization. In this study, some information related to the morphology and density of drops derived in primary and secondary atomization processes is reported. The experimental systems developed to examine primary and secondary atomization are schematically described in Figure 1.

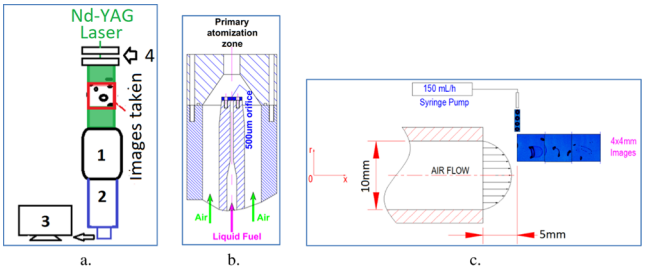

Figure 1. Schematics of the shadowgraph experiment setup (a) for observing the morphology of fuel fragments derived from primary atomization (b) and secondary atomization (c) (1: micro lens; 2: high-speed camera; 3: computer; and 4: diffusers).

A schematic of the shadowgraph imaging system is shown in Figure 1a. A high-speed camera was used in conjunction with a long-distance microscope objective lens (Questar, QM-100) to visualize a microscale of 4 × 4 mm^2 with a 512 × 512 pixel resolution. An Nd-YAG laser operated at 532 nm and 5 kHz was used as the high-speed light source. Two opal glass diffusing optics were used to remove laser coherence to provide a uniform source of illumination. This shadowgraph technique is a standard approach adopted for liquid atomization studies and this system has been used to investigate atomization and combustion characteristics of BF1−BF4 in our previous work.[23,25,58,66]

Figure 2b shows a centrally located air blast atomizer designed for the primary atomization study. A liquid fuel is injected through the 500 μm diameter orifice and the primary atomization of the liquid jet takes place with the aid of co-axial airflow. The fuel jet is then passed through a 10 mm diameter nozzle at the exit plane (see Figure 1b). The liquid jet's primary breakup takes place in the near-field of the nozzle exit under different airflow conditions (Weber number). The primary breakup process is captured using the backlit technique described in Figure 1a.

An air-cross flow system, shown schematically in Figure 1c, is adopted to study secondary atomization of fuel drops. This system consists of compressed air supplied to a minitunnel, which contains the final air discharge nozzle at its exit plane (see Figure 1c). Monodispersed droplets were slowly generated and delivered vertically to the cross-flow using a syringe pump and a needle with an internal diameter = 210 μm. The injection rate is kept constant at 150 mL/h. The mean diameter of the monodispersed droplets was measured using the long-distance microscope lens, shown in Figure 1a, providing an initial diameter equal to 400 μm (±5%) independent of the tested liquids. The observation reveals that the droplet generation process is driven by a Rayleigh dripping regime, where the droplet diameter $d \approx 1.89 \times$ ID. The breakup process of the monodispersed drops, known as secondary atomization, is driven by controlling the Weber number formulated at the nozzle exit.[16,58]

3. RESULTS AND DISCUSSION

3.1. Fuel Properties. *3.1.1. Heating Values.* One of the key properties used to evaluate the feasibility of utilizing a fuel for IC engines is the fuel heating or calorific value as the property directly determines the engine power output.

https://dx.doi.org/10.1021/acsomega.0c02083
ACS Omega 2020, 5, 20842−20853

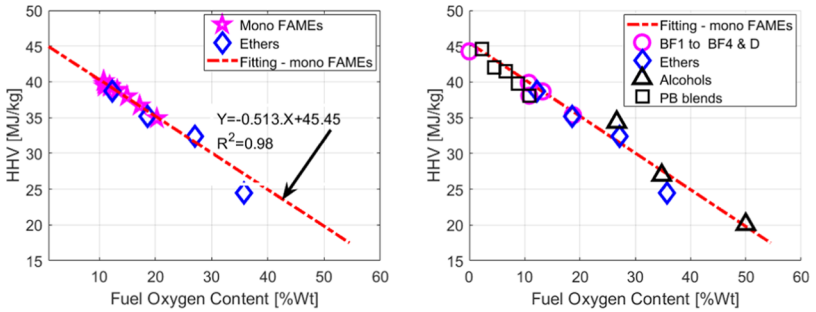

(a) Mono FAMEs & Ethers (b) BF1 to BF4 and PB blends

Figure 2. Correlation of higher heating values, HHVs, of 23 different oxygenated fuels and their oxygen content: (a) saturated mono-FAMEs (C8:0, C10:0, C12:0, C14:0, C16:0, and C18:0), unsaturated mono-FAMEs (C16:1, C18:1, C18:2, and C18:3), and ethers and (b) (i) diesel and four biodiesels, BF1−BF4; (ii) PB blends (B10, B20, B40, B60, and B100); (iii) ethers including diethylene glycol dimethyl ether, DGM(CH3O(CH2)2O(CH2)2OCH3), ethylene glycol mono-n-butyl ether, ENB (CH3(CH2)3O(CH2)2OH), 2-ethylhexyl acetate, EHA (CH3(CH2)7O(CO)CH3), and di-*n*-butyl ether, DBE (CH3CH2)3OCH3(CH2)3; and (iv) common alcohols, namely, methanol, ethanol, and butanol.

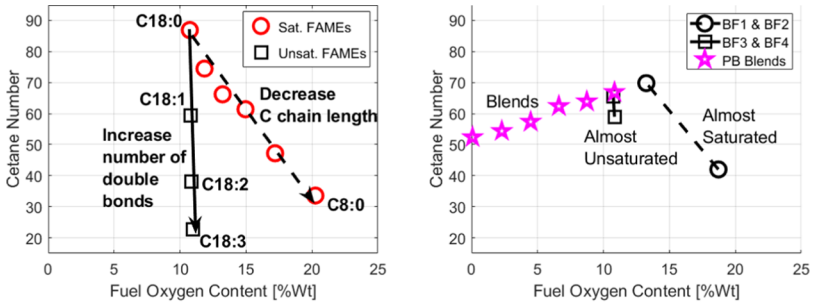

(a) Mono FAMEs (b) BF1 to BF4, and PB blends

Figure 3. Cetane numbers of mono-FAMEs and biodiesel blends versus their fuel oxygen content: (a) saturated FAMEs (C8:0−C18:0) and unsaturated FAMEs having 18 carbon atoms in their molecule (C18:1, C18:2, C18:3) and (b) biodiesels (BF1−BF4 and PB blends).

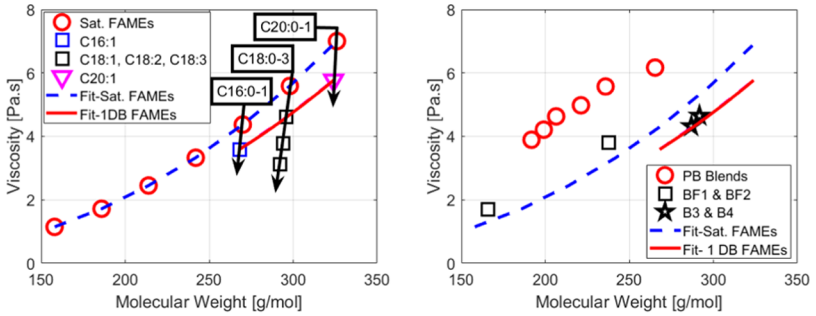

(a) Mono saturated & unsaturated FAMEs (b) Real biodiesels (BF1 to BF4) & PB blends

Figure 4. Viscosity of FAMEs and biodiesels versus their molecular weight: (a) saturated FAMEs (C8:0−C20:0) and unsaturated FAMEs (C16:2, C18:1, C18:2, C18:3, and C20:1) and (b) biodiesels (BF1−BF4 and PB blends).

Generally, the calorific value of a fuel is a function of its chemical compositions such as C, H, and O. Biodiesel constituents, FAMEs, have their chemical compositions, and consequently their heating values, varying in a broad range.

Higher heating values (HHVs) of six saturated FAMEs (C8:0, C10:0, C12:0, C14:0, C16:0, and C18:0), four unsaturated FAMEs (C16:1, C18:1, C18:2, and C18:3), and ethers are plotted versus their oxygen content by weight in Figure 1a. Similarly, HHVs of four pure biodiesels (BF1−BF4, respectively), six PB blends (B0, B10, B20, B40, B60, and B100), four ethers, and three alcohols are presented in Figure 2b. A linear fitting line is generated using the mono-FAMEs' HHV (shown in Figure 2a) and this line is plotted in both Figures 2a and 1b for comparison purposes.

Interestingly, the HHVs of the 23 fuels investigated here are almost inversely proportional to the fuel oxygen content, as clearly shown in Figure 1a,b. The outcome implies that the 98% confidence trend-line generated using mono-FAMEs' HHV data (shown in Figure 2a) could be a good reference when estimating the HHV for biodiesels and their blends, even esters and alcohols. The oxygen content in fuel is an "oxidizing agent" rather than a "fuel" and as such it enhances the combustion process while it decreases the HHV.[14,21] It is evident from Figure 1a,b that an increase from 10 to 20% in

https://dx.doi.org/10.1021/acsomega.0c02083
ACS Omega 2020, 5, 20842−20853

the oxygen content leads to a reduction of approximately 12% in HHV.

The observations obtained from Figure 1a,b could suggest a key to improving the calorific value for a certain biodiesel by decreasing its fuel oxygen content. This could be done by mixing the fuel with other biodiesels made from feedstock containing a high fraction of long-carbon-chain-length and/or high-saturated esters. This outcome obtained here could also be a good reference to estimate HHVs of biodiesels using their oxygen content.

3.1.2. Cetane Number. Cetane number (CN) is a dimensionless indicator of fuel ignition quality. CN is usually linked to the fuel ignition delay times or to the fuel reactivity. The reactivity of oxygenated fuels like biodiesels is a fuel property directly related to fuel oxygen content.[5,13,67,68] The cetane numbers of monosaturated and unsaturated FAMEs are shown in Figure 3a versus their oxygen content; similarly, the correlation of the fuel oxygen content and CN of biodiesels BF1−BF4 and PB blends is shown in Figure 3b.

It is evident from Figure 3a that an increase in the carbon chain length of saturated FAMEs (opposite direction of the continuous arrow shown in Figure 4a) leads to a significant decrease in the fuel oxygen content and this substantially increases the CN. An increase in the unsaturation degree (the continuous arrow shown in Figure 3a), in contrast, significantly decreases the fuels' CN. As the carbon chain length increases from C8:0 to C18:0, the CN of the saturated FAMEs increases almost three times, as shown in Figure 3a. When the number of double bonds increases from 0 to 3 (from C18:0 to C18:3), however, almost 75% reduction in CN is observed. It is noted that the variation in oxygen content of FAMEs having a similar carbon chain length (like C18 as an example in this case) is small and as such the influence of double bond function on the molecule decomposition and therefore on the fuel reactivity is significant and this was reported earlier in ref 69.

Figure 3b shows the CN of BF1−BF4 and a wide range of PB-diesel blends. Similar to the trends observed for the saturated and unsaturated FAMEs shown in Figure 3a, an increase in CN from BF1 to BF2 is observed and this is due to the longer carbon chain length of BF2 with respect to BF1 (see Table 1). As mentioned earlier, carbon chain lengths of BF3 and BF4 are close but BF3 is partially unsaturated, while BF4 is almost unsaturated, and this explains the lower CN of BF4 with respect to BF3, as clearly shown in Figure 3b.

It is also quite interesting that the CN of PB blends is almost linear with the blends' oxygen content. CN is a chemical property related directly to the combustion process, which is certainly very complex and as such the linear correlations between oxygen content and fuel CN shown in this figure should be interpreted with caution as other factors like H-abstraction, decomposition, and isomerization reaction also have significant roles in the fuel reactivity.

As discussed briefly in Section 1, the influence of molecular structures, including FAMEs as well as *n*-alkanes, on the high-temperature chemistry (HTC) is small; the difference in the fuels' reactivity could be attributed to the negative temperature chemistry (NTC) and/or low-temperature chemistry (LTC) characteristics of the fuels. In the LTC duration, H-abstractions occur followed by the decomposition processes to produce smaller radicals, which then isomerize to produce different species.[70] The isomerization is sensitive to both the size and number of double bonds contained in the fuel molecule. A recent comprehensive review in ref 71 reported that at low and intermediate temperatures, alkanes with longer paraffinic chain lengths involve more isomerization reactions, leading to their higher reactivity or shorter ignition delay time. Regarding the role of double bonds, Naik et al.[72] stated that the double bonds in FAMEs could inhibit certain low-temperature chain branching reaction pathways in which the double bond reduces the rates of radical isomerization reactions that normally accelerate the overall rate of LTC. Double bonds lower the low-temperature reaction rate by reducing both the number of secondary hydrogen atoms available for abstraction and the number of sites at which the six-member transition rings can form.[72] The study by Knothe[73] has noted a poorer oxidative stability for FAMEs with a higher number of double bonds in their carbon chain. The CH2 positions allylic to double bonds significantly affect the oxidation rate. For example, the relative oxidation rate is 1 for C18:1, 41 for C18:2, and up to 98 for C18:3.[5] This gives a further explanation for the dramatic decrease in CN from C18:1 to C18:3 observed in Figure 3.

3.1.3. Viscosity. The viscosities of monosaturated and unsaturated FAMEs versus their molecular weight are shown in Figure 4a. The dashed blue fitting curve is generated and shown in this figure for saturated FAMEs; similarly, the solid red fitting curve is for unsaturated FAMEs containing one double bond in their molecules (C16:1, C18:1, and C20:1). It is clear from this figure that exponential growths are observed for the CN of monosaturated FAMEs when increasing their chain length, and this is also true for FAMEs with one double bond.

Each of the three black solid arrows shown in Figure 4a represents the influence of the number of double bonds of mono-FAMEs having a similar carbon chain length on their CN. These three arrows correspond to C16, C18, and C20. These arrows show that among the FAMEs with similar carbon chain lengths, an increase in the number of double bonds significantly decreases the fuel viscosity. The viscosity of C18:3, for example, is just approximately half of that of C18:0.

The viscosity of FAMEs depends on their molecular geometries.[74] The tetrahedral bond angles on carbon result in a molecular geometry for saturated FAMEs (without double bond in the carbon chain) that is relatively linear although with zigzags. This molecular structure allows FAME molecules to be rather closely "stacked" together, resulting in strong intermolecular interactions. Unsaturated FAMEs containing one or more double bonds in the chain result in one or more "bends" in their molecules. These molecules do not "stack" very well. Therefore, the intermolecular interactions are much weaker than those of their saturated counterparts and this leads to their lower viscosity.

Correlations between the viscosity and molecular weight of biodiesels (BF1−BF4) and PB blends are shown in Figure 4b. The exponential trends of saturated FAMEs and one-double-bond FAMEs shown in Figure 4a are also included in Figure 4b for comparison purposes. It is shown in Figure 4b that viscosities of BF1 and BF2 (two saturated biodiesels with different carbon chain lengths) follow the monosaturated FAMEs' fitting curve (dashed blue), while viscosities of BF3 and BF4 are quite well placed on the one-double-bond FAMEs' fitting curve (solid red). BF2, owing to its higher carbon chain length and therefore higher molecular weight, is almost twice more viscous than BF1.

It is noted in Figure 4b (also reported in Table 1) that although having quite similar carbon chain lengths, BF4 with a

https://dx.doi.org/10.1021/acsomega.0c02083
ACS Omega 2020, 5, 20842−20853

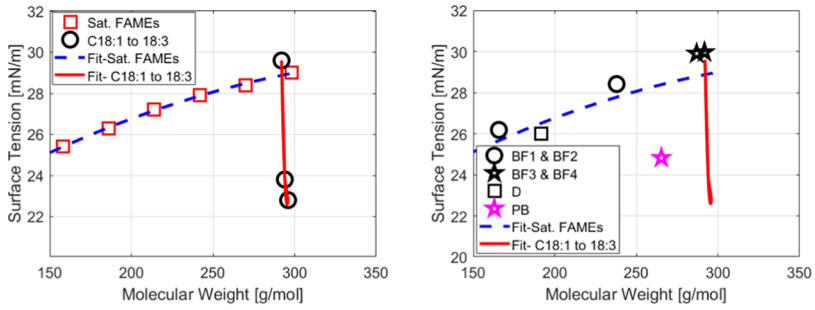

(a) Mono FAMEs (b) Real biodiesels (BF1 to BF4 & PB) and D

Figure 5. Surface tension values of (a) FAMEs: saturated FAMEs (C8:0−C18:0) and unsaturated FAMEs (C18:1, C18:2, and C18:3) and (b) real biodiesels (BF1−BF4 and PB) and diesel versus their molecular weight.

higher unsaturation degree has a high viscosity compared to that of BF3. There are a number of factors influencing FAMEs' viscosity, for example, carbon chain length, number of double bonds, position of double bonds, and types of double bonds (cis or trans).[74,75] Unfortunately, the influence of double bond positions and types has not been fully investigated in this study. As reported earlier in Table 1, the average number of C atoms of BF4 is a bit higher than that of BF3; BF4 contains both cis and trans C18:1, while BF3 has only cis C18:0. This could suggest for an examination of the influence of these factors on the viscosity of biodiesels in the future.

It is also noted in Figure 4b that the viscosity of PB blends does not follow the two fitting curves (saturated FAME curve and one-double-bond FAME curve). As mentioned earlier, a number of factors, including double bond positions and bond types (cis and trans), have not been investigated in this study. Also, the blend molecular weight, which is averaged using averaged molecular weights of pure diesel and PB and the blending ratio, may create some uncertainty. Nevertheless, the viscosity of PB blends is almost linear with the molecular weight. This is simply due to mixing a higher viscous liquid (PB in this case) and a lower viscous liquid (diesel in this case), and the blends' viscosity is a linear function of the blending ratio, which is proportional to the blends' molecular weight.

3.1.4. Surface Tension. The surface tension values of (i) monosaturated FAMEs and their fitting curve (dashed blue) and (ii) unsaturated FAMEs (C18:1−C18:3) are shown in Figure 5a versus their molecular weight. The two fitting curves shown in Figure 5a are for saturated FAMEs (dashed blue) and C18 FAMEs (solid red). These two fitting curves are also shown in Figure 5b where the surface tension values of BF1−BF4, PB, and diesel are shown. Surface tension values of the FAMEs reported in Figure 5a are taken from a previous study by Allen et al.[30]

Figure 5a shows that the surface tension values of the monosaturated FAMEs exponentially increase with the molecular weight. An increase in carbon chain length causes an increase in molecular weight and this leads to a significant increase in surface tension. In contrast, an increase in the number of double bonds from C18:1 to C18:3 leads to an approximately 25% reduction in the liquid's surface tension. As shown in Figure 5b, BF1 and BF2 follow the saturated FAMEs' fitting curve (dashed blue), while BF3 and BF4 are on the fitting curve of C18 FAMEs (solid red). Diesel shows its surface tension very close to that of methyl decanoate, C10:0 (shown in Figure 5a). Although PB contains 43.47% of C18:1 and 18.02% of C18:2, as shown in Table 1, the surface tension of PB does not follow the trend of C18:0−3, as shown in Figure 5b. This might be due to the influences of double bond position and double bond types (cis and trans) that have not been investigated in this study, as mentioned earlier.

Although the influence of saturated and unsaturated degrees on the surface tension of FAMEs and biodiesels is quite clear, as shown in Figure 5, it is noted here that the surface tension of the mono-FAMEs and biodiesels varies in a small range between 22 and 30 mN/m. It is well known that the viscosity of biodiesels produced from different feedstock varies as much as 100%, while their surface tension variation is from 5 to 10% approximately.[76]

According to the analysis provided in this section, a key to decrease the fuel viscosity and surface tension, two most important properties driving the fuel atomization process, is to add short-carbon-chain-length and/or low-unsaturation-degree (a small number of double bonds) FAMEs; however, this dramatically lowers the fuel reactivity and impairs their calorific value. An optimization study to obtain a balance between the carbon chain length and unsaturation degree of FAMEs in biodiesels could be useful as this may be a key to designing future biodiesels as well as to estimating properties of biodiesels manufactured from different feedstock and this in turn may help to improve energy utilization efficiency and decrease pollution. Optimization studies could particularly be useful for growing and producing the next generation of biodiesels derived from algae as the chemical profile of algae may be controlled by feeding the promising biomass.[77] Mixing biodiesels made from different feedstock could also be considered to balance the carbon chain length and unsaturation degree of the biodiesel. Mixing coconut-based biodiesel (saturated and medium carbon chain length, like BF2) and canola-based biodiesel (unsaturated and long carbon chain length, like BF4), for example, could help the mixture to have a reasonable heating value, cetane number, viscosity, and surface tension.

3.2. Morphology and Population of Liquid Fragments Formed in Primary and Secondary Atomization.

The atomization process depends mainly on the fuel's physical properties, including density, viscosity, and surface tension. It is well known that the variation in the density of biodiesels and their components is minimal. Demirbas[78] has shown that the density of biodiesels produced from common feedstock varies in a narrow gap of approximately 4%, from 848 to 885 kg/m^3. The small range of variation in biodiesel density discussed here and in biodiesel surface tension discussed in the previous

https://dx.doi.org/10.1021/acsomega.0c02083
ACS Omega 2020, 5, 20842−20853

section might be the reason why these physical properties are not specified in biodiesel standards ASTM-D6751 and EN14214. Therefore, the spray atomization quality mainly depends on the biodiesel viscosity.

The first author and his colleagues have developed a backlight experiment system to characterize the primary and secondary liquid breakup for different fuels and different nozzles.[23,58,79−81] An in-house Matlab image processor has also been developed and validated carefully for different spray conditions.[57,66,82] Figure 6 shows the morphology of liquid

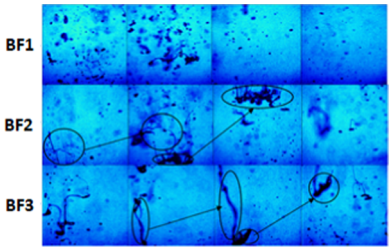

Figure 6. Morphology of biodiesel fragments formed in the primary atomization of an autoignited atomizer (frame size = 4 × 4 mm^2 corresponding to 532 × 532 pixels, camera frequency = 10 kHz, average fuel jet velocity = 64m/s and fuel *Re* = 43 000).

fragments derived at the nozzle exit plane of an autoignition burner when operating with biodiesels BF1, BF2, and BF3.[23,80] It was not possible to run BF4 in this burner due to its high viscosity. These images were taken at the nozzle exit plane under similar hydraulic conditions (jet velocity = 64m/s and liquid *Re* = 43 000). Each row represents one biodiesel indicated at the beginning of the row, while the four consecutive images shown in each column are taken in the exit plane of the nozzle under a camera's frequency of 10 kHz. Qualitatively, these biodiesels generated the same liquid structure. However, a quantitative analysis reported in our previous work[23] has noted that in the breakup zone (approximately five times of the nozzle diameter downstream), BF2 and BF3 generate a larger population of longer, stretched ligaments and this is attributable to their higher viscosity compared to that of BF1. Further downstream, where the breakup process is completed, the liquid fragment densities are very similar among the biodiesels tested.

Also using the backlight imaging technique, secondary atomization characteristics of droplets of four biodiesels (BF1 to BF4) were examined in an air-cross flow system. In the system, biodiesel constant diameter drops are generated slowly using a drop generator.[58] The drops fall down freely under gravity into a horizontal airflow. The airflows can be controlled to break up the drops under a wide range of Weber numbers from 20 to 400. Details about this setup can be found in ref 16.

Differences in the secondary atomization of different biodiesels could be expected as the breakup time is a function of physical properties, especially surface tension and viscosity,[83] which vary from one biodiesel to another. However, the breakup mechanisms observed for the four biodiesels tested here are somewhat similar according to the morphology of the liquid fragments observed. Therefore, examples of breakup morphology are shown in Figure 7 only for fuel BF4. Although the morphology of the secondary breakup regimes has been described in detail in the literature, it is difficult to quantify the relative occurrence of a particular fluid shape, especially when different fuels are used. The reader is directed to ref 16 for further information related to breakup morphology .

A quantitative analysis of the population of small drops formed in the breakup zone of the secondary atomization system is given in Figure 8. The small drops here include all fragments having an aspect ratio (ratio of major to minor axis) smaller than 3 and the mean of major and minor axis smaller than 150 μm.[16] The probability here is computed simply using the fraction of small drops over the total fragments observed. It is shown from Figure 8 that close to the initial breakup location (x/D = 0,[16] where D is the nozzle diameter), some differences are noted for these biodiesels. However, downstream where x/D exceeds 1.7, the population of small drops

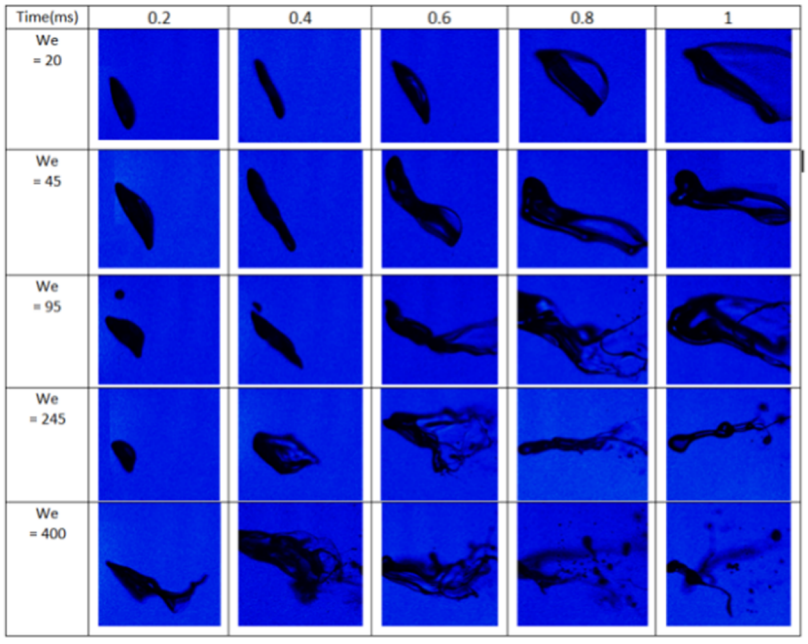

Figure 7. Morphology of drop breakup in a secondary atomization laboratory system (cross-flow system).

https://dx.doi.org/10.1021/acsomega.0c02083
ACS Omega 2020, 5, 20842−20853

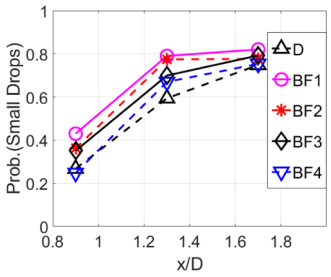

Figure 8. Probability of the small drops of four biodiesels (BF1, BF2, BF3, and BF4) and diesel at We = 245 versus the axial location, x/D, where D is the nozzle diameter.

generated is very similar among the biodiesels tested. This achievement is in good agreement with the primary breakup characteristic discussed above.

3.3. Drop Evaporation. In this section, the evaporation rate is calculated for FAMEs using the D-square model.[35] In this model, an ambient temperature (Ti) of 850 K and an initial droplet diameter of 100 μm are taken. Although the initial droplet diameter chosen in this study is quite big compared to that of droplets in diesel engines, the choice has its own purpose, which is to be equivalent to droplet sizes in fundamental studies of primary and secondary atomization done previously in laboratory burners and atomizers by the first author.[25] Some information of fuel atomization was briefly provided in the previous section. Furthermore, the choice of droplet size would not change the trend in evaporation rates. FAMEs used in this study are common components of biodiesels manufactured from different feedstock; they include eight monosaturated FAMEs (C12:0, C14:0, C16:0, C17:0, C18:0, C20:0. C22:0, and C24:0) and seven monounsaturated FAMEs (C16:1, C18:1, C18:2, C18:3, C20:1, C22:1, and C24:1). The thermophysical properties of the liquids that are needed to input the D-square model can be estimated using the databases and models presented elsewhere.[5,32,33,84]

Figure 9 shows a correlation between the droplet lifetime of saturated and unsaturated FAMEs and their fuel oxygen

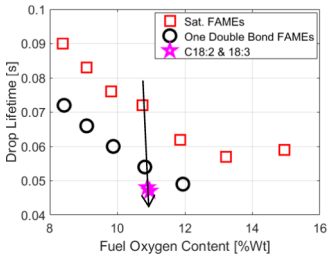

Figure 9. Droplet lifetime of mono-FAMEs versus their oxygen content (initial conditions: drop diameter, d_0 = 100 μm, and Ti = 850 K).

content. It is clear from the figure that both carbon chain length and number of double bonds in the chain (see the square red symbols shown in Figure 9) have strong effects on the droplet lifetime. It is notable that when the carbon chain length of saturated FAMEs increases, their drop lifetime increases significantly. This trend is also true for the one-double-bond FAMEs investigated here (C16:1, C18:1, C20:1, C22:1, and C24:1).

Regarding the influence of the number of double bonds, the solid black arrow shown in Figure 9 indicates the effect of the number of double bonds of C18:0, C18:1, C18:2, and C18:3 on their evaporation rate. Although the number of double bonds has a little effect on the FAMEs' oxygen content, it is evident that the double bond number significantly affects the droplet lifetime. When the number of double bonds increases from 0 to 3 in the case of C18, the droplet lifetime reduces almost 40%, as shown in Figure 9. Along with the findings provided in previous sections that the fuel reactivity increases with increasing carbon chain length and/or saturation degree, the observation on the correlation of drop lifetime versus carbon FAME molecular profiles here may suggest that the difference in autoignition characteristics among biodiesels with different molecular structures could be due to chemical processes (high-, negative-, or low-temperature autoignition) rather than physical ones, and this would suggest a useful work in the future to investigate the effect of biodiesel molecular structures on physical and chemical autoignition characteristics.

Droplet lifetime significantly depends on the fuel specific heat capacity, C_p, and heat of evaporation, h_{fg}. In the D-square law, these two properties are used to compute the Spalding number. The correlation of the C_p of FAMEs and their oxygen content is shown in Figure 10a; similarly, Figure 10b shows the correlation of h_{fg} and the oxygen content of FAMEs. An opposite trend between C_p and h_{fg} is noted, as shown in Figure 10a,b. Since an increase in oxygen content leads to an increase in h_{fg} (opposite to the droplet lifetime trend shown in Figure 9), the trend in drop lifetime shown in Figure 9 is driven by the trend in specific heat capacity.

A short but important note for the correlations between the number of double bonds/carbon chain length and specific heat capacity has been provided in ref 85 and our observations presented above agree well with this note. The double bonds present in FAME molecules decrease the vibrations of carbon atoms adjacent to the bonds. The decrease in vibrations of the two hydrogen atoms replaced by the double bonds might be attributable to the decrease in specific heat capacity. It was also reported earlier that the formation of double bonds results in increased fluidity and volatility of methyl esters and this leads to decreased specific heat capacity.[86] Additionally, different FAME molecular structures (e.g., functional groups such as ═CH in cis-double bond, aliphatic CH2, aliphatic CH3, free fatty acids, and C═C in olefins) result in different vibration modes and this has been discussed quite clearly in ref 86.

4. CONCLUSIONS

An extensive analysis has been carried out in this study to examine biodiesels produced from different feedstock and mono-fatty-acid methyl esters. It shows that the influence of fuel molecular profile (oxygen content, carbon chain length, and number of double bonds) on fuel physical and chemical properties (heating value, cetane number, viscosity, and surface tension) as well as thermal properties (specific heat capacity and heat of evaporation) is significant. The oxygen content in a biodiesel is directly linked to the carbon chain length and number of double bonds in the fuel molecules and the following conclusions could be drawn:

(i) An increase in oxygen content significantly decreases biodiesel heating values but enhances the fuel reactivity (cetane number). Correlations between oxygen content and fuel properties are observed for both FAMEs and biodiesels but they need to be carefully accounted for

https://dx.doi.org/10.1021/acsomega.0c02083
ACS Omega 2020, 5, 20842−20853

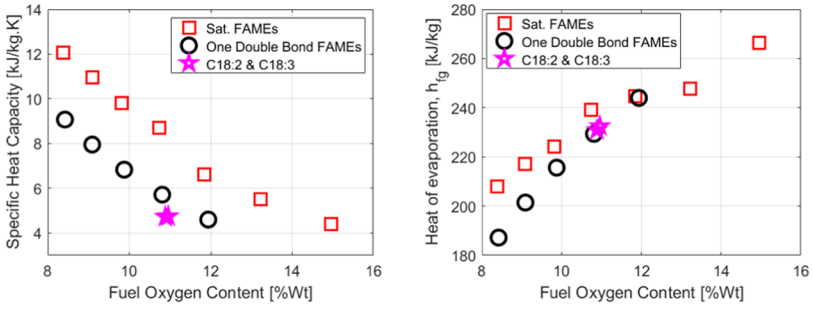

(a) Specific heat capacity – C_p of FAMEs (b) Heat of evaporation - h_{fg} of FAMEs

Figure 10. (a) Specific heat capacity, C_p, and (b) heat of evaporation, h_{fg}, of FAMEs versus oxygen content.

the carbon chain length and number of double bonds in the fuel molecules when interpreting.

(ii) At the breakup zone (e.g., close to the nozzle exit), the influence of fuel properties, especially viscosity, on the morphology and density of fuel fragments formed in the zone is quite clear; however, downstream, where the breakup is completed, this influence is minimal.

(iii) The thermal properties (specific heat capacity and heat of evaporation) have strong effects on fuel drop evaporation.

(iv) The correlations between fuel molecular structure and (i) fuel reactivity and (ii) atomization and evaporation may suggest that the difference in autoignition characteristics among biodiesels with different molecular structures could be due to chemical processes (high-, negative-, or low-temperature autoignition) rather than physical ones, and this would suggest a useful work in the future to investigate the effect of biodiesel molecular structures on physical and chemical autoignition characteristics.

AUTHOR INFORMATION

Corresponding Author

Phuong X. Pham − *Faculty of Vehicle & Energy Engineering, Le Quy Don Technical University, Hanoi 10000, Vietnam;* orcid.org/0000-0002-0726-5808; Email: phuongpham@lqdtu.edu.vn

Authors

Kien T. Nguyen − *Faculty of Vehicle & Energy Engineering, Le Quy Don Technical University, Hanoi 10000, Vietnam*

Thin V. Pham − *Faculty of Physical and Chemical Engineering, Le Quy Don Technical University, Hanoi 10000, Vietnam*

Vu H. Nguyen − *Faculty of Vehicle & Energy Engineering, Le Quy Don Technical University, Hanoi 10000, Vietnam*

Complete contact information is available at: https://pubs.acs.org/10.1021/acsomega.0c02083

Author Contributions

The manuscript was written through the contributions of all authors. All authors have given approval to the final version of the manuscript. The authors contributed equally.

Notes

The authors declare no competing financial interest.

ACKNOWLEDGMENTS

This work is financially supported by the National Foundation for Science Technology Development (NAFOSTED) under grant number 107.01-2018.310.

REFERENCES

(1) Maceiras, R.; Rodrı, M.; Cancela, A.; Urréjola, S.; Sánchez, A. Macroalgae: raw material for biodiesel production. *Appl. Energy* **2011**, *88*, 3318−3323.

(2) Pham, P.; Vo, D.; Jazar, R. Development of fuel metering techniques for spark ignition engines. *Fuel* **2017**, *206*, 701−715.

(3) Watson, H. C.; Phuong, P. X. In *Why Liquid Phase LPG Port Injection has Superior Power and Efficiency to Gas Phase Port Injection*, SAE Technical Paper, 2007.

(4) Phuong, P. X. In *An Experimental Strategy for the Manufacture of Aviation Fuel*, SAE Technical Paper, 2010.

(5) Krahl, J.; Knothe, G.; Van Gerpen, J. H. *Biodiesel Handbook*; AOCS Press, 2010.

(6) Wilcox, J. Grand challenges in advanced fossil fuel technologies. *Front. Energy Res.* **2014**, *2*, No. 47.

(7) Reitz, R. D. Grand challenges in engine and automotive engineering *Front. Mech. Eng.* 2015, *1*:1, DOI: 10.3389/fmech.2015.00001.

(8) Secretariat, O. *2017 OPEC World Oil Outlook*; Organization of the Petroleum Exporting Countries, 2017.

(9) Ashok, B.; Nanthagopal, K.; Anand, V.; Aravind, K.; Jeevanantham, A.; Balusamy, S. Effects of n-octanol as a fuel blend with biodiesel on diesel engine characteristics. *Fuel* **2019**, *235*, 363−373.

(10) Nanthagopal, K.; Ashok, B.; Saravanan, B.; Korah, S. M.; Chandra, S. Effect of next generation higher alcohols and Calophyllum inophyllum methyl ester blends in diesel engine. *J. Cleaner Prod.* **2018**, *180*, 50−63.

(11) Knothe, G. Biodiesel and renewable diesel: a comparison. *Prog. Energy Combust. Sci.* **2010**, *36*, 364−373.

(12) Dec, J. E. A conceptual model of DL diesel combustion based on laser-sheet imaging. *SAE Trans.* **1997**, 1319−1348.

(13) Westbrook, C. K. Biofuels combustion. *Annu. Rev. Phys. Chem.* **2013**, *64*, 201−219.

(14) Pham, P. X.; Bodisco, T. A.; Ristovski, Z. D.; Brown, R. J.; Masri, A. R. The influence of fatty acid methyl ester profiles on inter-cycle variability in a heavy duty compression ignition engine. *Fuel* **2014**, *116*, 140−150.

(15) Odibi, C.; Babaie, M.; Zare, A.; Nabi, M. N.; Bodisco, T. A.; Brown, R. J. Exergy analysis of a diesel engine with waste cooking biodiesel and triacetin. *Energy Convers. Manage.* **2019**, *198*, No. 111912.

(16) Pham, X. P. *Influences of Molecular Profiles of Biodiesels on Atomization, Combustion and Emission Characteristics*; The University of Sydney, 2014.

(17) Yan, J.; Chisti, Y. Energy from algae: Current status and future trends. *Appl. Energy* **2011**, *88*, 282.

(18) Lapuerta, M.; Armas, O.; Rodriguez-Fernandez, J. Effect of biodiesel fuels on diesel engine emissions. *Prog. Energy Combust. Sci.* **2008**, *34*, 198−223.
(19) Hoekman, S. K.; Robbins, C. Review of the effects of biodiesel on NOx emissions. *Fuel Process. Technol.* **2012**, *96*, 237−249.
(20) Miyamoto, N.; Ogawa, H.; Nurun, N. M.; Obata, K.; Arima, T. Smokeless, low NOx, high thermal efficiency, and low noise diesel combustion with oxygenated agents as main fuel. *SAE Trans.* **1998**, 171−177.
(21) Nguyen, V. H.; Pham, P. X. Biodiesels: Oxidizing enhancers to improve CI engine performance and emission quality. *Fuel* **2015**, *154*, 293−300.
(22) Ragland, K. W.; Bryden, K. M. *Combustion Engineering*; CRC Press, 2011.
(23) Kourmatzis, A.; Pham, P. X.; Masri, A. R. Air assisted atomization and spray density characterization of ethanol and a range of biodiesels. *Fuel* **2013**, *108*, 758−770.
(24) Mueller, C. J.; Musculus, M.; Pickett, L. M.; Pitz, W. J.; Westbrook, C. K. *The Oxygen Ratio: A Fuel-Independent Measure of Mixture Stoichiometry*; Lawrence Livermore National Lab.(LLNL): Livermore, CA (United States), 2003.
(25) Pham, P. X.; Kourmatzis, A.; Masri, A. R. In *Spray Characterization of Ethanol and Saturated Biodiesels of Different Carbon Chain Lengths*, Proceedings of the Australian Combustion Symposium; The Combustion Institute Australian and New Zealand Section, 2013.
(26) Allen, C.; Watts, K. Comparative analysis of the atomization characteristics of fifteen biodiesel fuel types. *Trans. ASAE* **2000**, *43*, 207.
(27) Kostas, J.; Honnery, D.; Soria, J. A correlation image velocimetry-based study of high-pressure fuel spray tip evolution. *Exp. Fluids* **2011**, *51*, No. 667.
(28) Pham, P. X.; Pham, N. V.; Vu, L. D.; Nguyen, K. T.; Pham, T. V.; Nguyen, V. H.; Luong, T. D.; Nguyen, M. Q. In *Development of a Backlight Imaging System to Investigate Liquid Breakup in Near-Field Swirl Atomizer*, International Conference on Engineering Research and Applications; Springer, 2019.
(29) Guildenbecher, D.; López-Rivera, C.; Sojka, P. Secondary atomization. *Exp. Fluids* **2009**, *46*, 371.
(30) Allen, C. A.; Watts, K. C.; Ackman, R. G. Predicting the surface tension of biodiesel fuels from their fatty acid composition. *J. Am. Oil Chem. Soc.* **1999**, *76*, 317−323.
(31) Reid, R. C.; Prausnitz, J. M.; Poling, B. E. *The Properties of Gases and Liquids*, **1987**, United States.
(32) Sazhin, S.; Al Qubeissi, M.; Kolodnytska, R.; Elwardany, A.; Nasiri, R.; Heikal, M. Modelling of biodiesel fuel droplet heating and evaporation. *Fuel* **2014**, *115*, 559−572.
(33) Al Qubeissi, M.; Sazhin, S.; Crua, C.; Turner, J.; Heikal, M. Modelling of biodiesel fuel droplet heating and evaporation: Effects of fuel composition. *Fuel* **2015**, *154*, 308−318.
(34) Ahmed, T.; Kourmatzis, A.; Pham, P.; Masri, A. Droplet evaporation modeling of electrified fatty acid methyl esters. *Fuel* **2018**, *231*, 244−252.
(35) Stephen, R. T. *An Introduction to Combustion: Concepts and Applications*, 3rd ed.; McGraw-Hill, 2012.
(36) Fattah, I. M. R.; Ming, C.; Chan, Q.; Wehrfritz, A.; Pham, P.; Yang, W.; Kook, S.; Medwell, P.; Yeoh, G.; Hawkes, E.; Masri, A. R. Spray and combustion investigation of post injections under low-temperature combustion conditions with biodiesel. *Energy Fuels* **2018**, *32*, 8727−8742.
(37) Zhang, R.; Pham, P. X.; Kook, S.; Masri, A. R. Influence of biodiesel carbon chain length on in-cylinder soot processes in a small bore optical diesel engine. *Fuel* **2019**, *235*, 1184−1194.
(38) McCormick, R. L.; Westbrook, S. R. Storage stability of biodiesel and biodiesel blends. *Energy Fuels* **2010**, *24*, 690−698.
(39) Suraj, C.; Krishnasamy, A.; Sundararajan, T. Investigations on Gradual and Accelerated Oxidative Stability of Karanja Biodiesel and Biodiesel−Diesel Blends. *Energy Fuels* **2019**, *33*, 9196−9204.
(40) Casas, A.; Ruiz, J. R.; Ramos, M.a.J.s.; Pérez, A. Effects of triacetin on biodiesel quality. *Energy Fuels* **2010**, *24*, 4481−4489.
(41) Pratas, M. J.; Freitas, S. V.; Oliveira, M. B.; Monteiro, S. C.; Lima, ÁS.; Coutinho, J. A. Biodiesel density: Experimental measurements and prediction models. *Energy Fuels* **2011**, *25*, 2333−2340.
(42) Ooi, J. B.; Yap, J.-H.; Tran, M.-V.; Leong, J. C. K. Experimental Investigation on the Droplet Burning Behavior of Diesel−Palm Biodiesel Blends. *Energy Fuels* **2019**, *33*, 11804−11811.
(43) Li, A.; Yu, L.; Lu, X.; Huang, Z.; Zhu, L. Experimental and Modeling Study on Autoignition of a Biodiesel/n-Heptane Mixture and Related Surrogate in a Heated Rapid Compression Machine. *Energy Fuels* **2019**, *33*, 4552−4563.
(44) Jayabal, R.; Thangavelu, L.; Velu, C. Experimental Investigation on the Effect of Ignition Enhancers in the Blends of Sapota Biodiesel/Diesel Blends on a CRDi Engine. *Energy Fuels* **2019**, *33*, 12431−12440.
(45) Tinprabath, P.; Hespel, C.; Chanchaona, S.; Foucher, F. Influence of biodiesel and diesel fuel blends on the injection rate under cold conditions. *Fuel* **2015**, *144*, 80−89.
(46) Karthickeyan, V.; Thiyagarajan, S.; Ashok, B.; Geo, V. E.; Azad, A. Experimental investigation of pomegranate oil methyl ester in ceramic coated engine at different operating condition in direct injection diesel engine with energy and exergy analysis. *Energy Convers. Manage.* **2020**, *205*, No. 112334.
(47) Ming, C.; Fattah, I. R.; Chan, Q. N.; Pham, P. X.; Medwell, P. R.; Kook, S.; Yeoh, G. H.; Hawkes, E. R.; Masri, A. R. Combustion characterization of waste cooking oil and canola oil based biodiesels under simulated engine conditions. *Fuel* **2018**, *224*, 167−177.
(48) Agarwal, A. K.; Gupta, T.; Shukla, P. C.; Dhar, A. Particulate emissions from biodiesel fuelled CI engines. *Energy Convers. Manage.* **2015**, *94*, 311−330.
(49) Bragadeshwaran, A.; Kasianantham, N.; Balusamy, S.; Muniappan, S.; Reddy, D. M. S.; Subhash, R. V.; Pravin, N. A.; Subbarao, R. Mitigation of NOx and smoke emissions in a diesel engine using novel emulsified lemon peel oil biofuel. *Environ. Sci. Pollut. Res.* **2018**, *25*, 25098−25114.
(50) Thiyagarajan, S.; Edwin Geo, V.; Ashok, B.; Nanthagopal, K.; Vallinayagam, R.; Saravanan, C. G.; Kumaran, P. NOx emission reduction using permanent/electromagnet-based fuel reforming system in a compression ignition engine fueled with pine oil. *Clean Technol. Environ. Policy* **2019**, *21*, 815−825.
(51) Ashok, B.; Nanthagopal, K.; Mohan, A.; Johny, A.; Tamilarasu, A. Comparative analysis on the effect of zinc oxide and ethanox as additives with biodiesel in CI engine. *Energy* **2017**, *140*, 352−364.
(52) Ashok, B.; Nanthagopal, K.; Jeevanantham, A.; Bhowmick, P.; Malhotra, D.; Agarwal, P. An assessment of calophyllum inophyllum biodiesel fuelled diesel engine characteristics using novel antioxidant additives. *Energy Convers. Manage.* **2017**, *148*, 935−943.
(53) Ashok, B.; Nanthagopal, K.; Subbarao, R.; Johny, A.; Mohan, A.; Tamilarasu, A. Experimental studies on the effect of metal oxide and antioxidant additives with Calophyllum Inophyllum Methyl ester in compression ignition engine. *J. Cleaner Prod.* **2017**, *166*, 474−484.
(54) Sani, S.; Kaisan, M.; Kulla, D.; Obi, A.; Jibrin, A.; Ashok, B. Determination of physico chemical properties of biodiesel from Citrullus lanatus seeds oil and diesel blends. *Ind. Crops Prod.* **2018**, *122*, 702−708.
(55) Pourkhesalian, A.; Stevanovic, S.; Salimi, F.; Rahman, M.; Wang, H.; Pham, P.; Bottle, S.; Masri, A.; Brown, R.; Ristovski, Z. Influence of fuel molecular structure on the volatility and oxidative potential of biodiesel particulate matter. *Environ. Sci. Technol.* **2014**, *48*, 12577−12585.
(56) www.pgchemicals.com.
(57) Pham, P.; Kourmatzis, A.; Masri, A. Local characteristics of fragments in atomizing sprays. *Exp. Therm. Fluid Sci.* **2018**, *95*, 44−51.
(58) Pham, P.; Kourmatzis, A.; Masri, A. In *Secondary Atomization Characteristics of Biofuels with Different Physical Properties*, 19th Australasian Fluid Mechanics Conference, AFMC 2014; Australasian Fluid Mechanics Society, 2014.

https://dx.doi.org/10.1021/acsomega.0c02083
ACS Omega 2020, 5, 20842−20853

(59) Nguyen, V. H.; Vu, H.; DO, H. M.; Woo, J.; Jun, H. H. Esterification of waste fatty acid from palm oil refining process into biodiesel by heterogeneous catalysis: Fuel properties of B10, B20 blends. *Int. J. Renewable Energy Environ. Eng.* **2013**, *1*, 1−5.
(60) Pham, P. X.; Nguyen, V. H. Residue-Based Biodiesel: Experimental Investigation into Engine Combustion and Emission Formation. *J. Energy Eng.* **2017**, *143*, No. 04017047.
(61) Hoang, V. N.; Thi, L. D. Experimental study of the ignition delay of diesel/biodiesel blends using a shock tube. *Biosyst. Bioeng.* **2015**, *134*, 1−7.
(62) Pham, P.; Bodisco, T. A.; Stevanovic, S.; Rahman, M.; Wang, H.; Ristovski, Z.; Brown, R.; Masri, A. Engine performance characteristics for biodiesels of different degrees of saturation and carbon chain lengths. *SAE Int. J. Fuels Lubr.* **2013**, *6*, 188−198.
(63) Jahirul, M. I.; Senadeera, W.; Brooks, P.; Brown, R. J.; Situ, R.; Pham, P. X.; Masri, A. R. In *An Artificial Neutral Network (ANN) Model for Predicting Biodiesel Kinetic Viscosity as a Function of Temperature and Chemical Compositions*, MODSIM2013, 20th International Congress on Modelling and Simulation; Modelling and Simulation Society of Australia and New Zealand, 2013.
(64) Bodisco, T. A.; Pham, P. X.; Islam, M.; Brown, R. J.; Masri, A. R.; Bockhorn, H. In *Ignition Delay of Bio-Fuels in a Common-Rail Compression Ignition Engine*, Proceedings of The Australian Combustion Symposium Nov 6−8; Combustion Institute, 2013.
(65) Wang, M.*The Green House Gases, Regulated Emissions, and Energy Use in Transportation (GREET) Model: Version 1.5*; Center for Transportation Research, Argonne National Laboratory, 2008.
(66) Kourmatzis, A.; Pham, P. X.; Masri, A. R. A two-angle far-field microscope imaging technique for spray flows. *Meas. Sci. Technol.* **2017**, *28*, No. 035302.
(67) Duong, M. Q.; Nguyen, V. H.; Pham, P. X. In *Development of Empirical Correlations for Ignition Delay in a Single Cylinder Engine Fueled with Diesel/Biodiesel Blends*, 2019 International Conference on System Science and Engineering (ICSSE); IEEE, 2019; p 614.
(68) Bodisco, T. A.; Pham, P. X.; Islam, A.; Brown, R. J.; Masri, A. R.; Bockhorn, H. In *Ignition Delay of Bio-Fuels in a Common-Rail Compression Ignition Engine*, Proceedings of the Australian Combustion Symposium, 2013.
(69) Schönborn, A.; Ladommatos, N.; Williams, J.; Allan, R.; Rogerson, J. The influence of molecular structure of fatty acid monoalkyl esters on diesel combustion. *Combust. Flame* **2009**, *156*, 1396−1412.
(70) Westbrook, C. K. Chemical kinetics of hydrocarbon ignition in practical combustion systems. *Proc. Combust. Inst.* **2000**, *28*, 1563−1577.
(71) Boot, M. D.; Tian, M.; Hensen, E. J.; Sarathy, S. M. Impact of fuel molecular structure on auto-ignition behavior−Design rules for future high performance gasolines. *Prog. Energy Combust. Sci.* **2017**, *60*, 1−25.
(72) Naik, S. N.; Goud, V. V.; Rout, P. K.; Dalai, A. K. Production of first and second generation biofuels: a comprehensive review. *Renewable Sustainable Energy Rev.* **2010**, *14*, 578−597.
(73) Knothe, G. Improving biodiesel fuel properties by modifying fatty ester composition. *Energy Environ. Sci.* **2009**, *2*, 759−766.
(74) McKee, T.; McKee, J. *Biochemistry: The Molecular Basis of Life*, 5th ed.; Oxford University Press: New York, 2011.
(75) Knothe, G.; Steidley, K. R. Kinematic viscosity of biodiesel fuel components and related compounds. Influence of compound structure and comparison to petrodiesel fuel components. *Fuel* **2005**, *84*, 1059−1065.
(76) Herbinet, O.; Pitz, W. J.; Westbrook, C. K. Detailed chemical kinetic oxidation mechanism for a biodiesel surrogate. *Combust. Flame* **2008**, *154*, 507−528.
(77) Demirbas, A.; Demirbas, M. F. Algae Energy: Algae as a New Source of Biodiesel. In *Green Energy and Technology*; Springer Science & Business Media, 2010.
(78) Demirbas, A. Comparison of transesterification methods for production of biodiesel from vegetable oils and fats. *Energy Convers. Manage.* **2008**, *49*, 125−130.
(79) Kourmatzis, A.; Pham, P.; Pandey, P. In *Initial Characterisation of an Auto-Ignition Burner with Dense Spray Boundary Conditions*, Mediterranean Combustion Symposium (8th: 2013); The Combustion Institute, 2013.
(80) Kourmatzis, A.; Pham, P. X.; Masri, A. R. Characterization of atomization and combustion in moderately dense turbulent spray flames. *Combust. Flame* **2015**, *162*, 978−996.
(81) Singh, G.; Pham, P.; Kourmatzis, A.; Masri, A. Effect of electric charge and temperature on the near-field atomization of diesel and biodiesel. *Fuel* **2019**, *241*, 941−953.
(82) Pham, P. X.; Kourmatzis, A.; Masri, A. R. Simultaneous volume-velocity measurements in the near field of atomizing sprays. *Meas. Sci. Technol.* **2017**, *28*, No. 115203.
(83) Faeth, G.; Hsiang, L.-P.; Wu, P.-K. Structure and breakup properties of sprays. *Int. J. Multiphase Flow* **1995**, *21*, 99−127.
(84) Zong, L.; Ramanathan, S.; Chen, C.-C. Predicting thermo-physical properties of mono-and diglycerides with the chemical constituent fragment approach. *Ind. Eng. Chem. Res.* **2010**, *49*, 5479−5484.
(85) Zhu, X.; Phinney, D. M.; Paluri, S.; Heldman, D. R. Prediction of liquid specific heat capacity of food lipids. *J. Food Sci.* **2018**, *83*, 992−997.
(86) Anand, K.; Sharma, R.; Mehta, P. S. A comprehensive approach for estimating thermo-physical properties of biodiesel fuels. *Appl. Therm. Eng.* **2011**, *31*, 235−242.

https://dx.doi.org/10.1021/acsomega.0c02083
ACS Omega 2020, 5, 20842−20853